

Detection of neural connections with *ex vivo* MRI using a ferritin-encoding trans-synaptic virus

Ning Zheng^{a,b,1}, Peng Su^{c,1}, Yue Liu^a, Huadong Wang^a, Binbin Nie^{b,d}, Xiaohui Fang^a, Yue Xu^a, Kunzhang Lin^a, Pei Lv^a, Xiaobin He^a, Yi Guo^a, Baoci Shan^{b,d,e}, Anne Manyande^f, Jie Wang^{a,b,**}, Fuqiang Xu^{a,b,c,e,*}

^a State Key Laboratory of Magnetic Resonance and Atomic and Molecular Physics, Key Laboratory of Magnetic Resonance in Biological Systems, Wuhan Center for Magnetic Resonance, Wuhan Institute of Physics and Mathematics, Chinese Academy of Sciences, Wuhan, 430071, PR China

^b University of Chinese Academy of Sciences, Beijing, 100049, PR China

^c Wuhan National Laboratory for Optoelectronics, Huazhong University of Science and Technology, Wuhan, 430074, PR China

^d Key Laboratory of Nuclear Radiation and Nuclear Energy Technology, Institute of High Energy Physics, Chinese Academy of Sciences, Beijing, 100049, PR China

^e Center for Excellence in Brain Science and Intelligent Technology, Chinese Academy of Sciences, Shanghai, 200031, PR China

^f School of Human and Social Sciences, University of West London, London, UK

ARTICLE INFO

Keywords:

Ferritin
Synaptically connected neural networks
MRI
Fluorescent imaging
VSV

ABSTRACT

The elucidation of neural networks is essential to understanding the mechanisms of brain functions and brain disorders. Neurotropic virus-based trans-synaptic tracing tools have become an effective method for dissecting the structure and analyzing the function of neural-circuitry. However, these tracing systems rely on fluorescent signals, making it hard to visualize the panorama of the labeled networks in mammalian brain *in vivo*. One MRI method, Diffusion Tensor Imaging (DTI), is capable of imaging the networks of the whole brain in live animals but without information of anatomical connections through synapses. In this report, a chimeric gene coding for ferritin and enhanced green fluorescent protein (EGFP) was integrated into Vesicular stomatitis virus (VSV), a neurotropic virus that is able to spread anterogradely in synaptically connected networks. After the animal was injected with the recombinant VSV (rVSV), rVSV-Ferritin-EGFP, into the somatosensory cortex (SC) for four days, the labeled neural-network was visualized in the postmortem whole brain with a T2-weighted MRI sequence. The modified virus transmitted from SC to synaptically connected downstream regions. The results demonstrate that rVSV-Ferritin-EGFP could be used as a bimodal imaging vector for detecting synaptically connected neural-network with both *ex vivo* MRI and fluorescent imaging. The strategy in the current study has the potential to longitudinally monitor the global structure of a given neural-network in living animals.

1. Introduction

The extremely complex neural circuit is the structural basis for all brain functions, such as consciousness, cognition, emotion, learning and memory. Therefore, identifying and dissecting the corresponding neural-circuit for a given function is a prerequisite for understanding the basic function of the brain and the cause of neurological disorders (Tye and Deisseroth, 2012).

Currently, there are a few approaches that can be used to investigate

the structure of neural circuits (Lerner et al., 2016). Firstly, neural-circuit tracers, which can be efficiently taken up and actively transported by neurons, have long been utilized to dissect the neural network. These tracers include horseradish peroxidase (Paton and Nottebohm, 1984), fluoro-gold (Brog et al., 1993), wheat germ agglutinin (Numan and Numan, 1997), tetanus cholera B fragment (Lai et al., 2015), barley lectin (Horowitz et al., 1999) and neurotropic viruses (Callaway, 2008; Enquist and Card, 2003). Among these tracer-based methods, the method based on engineered neurotropic viral vectors has made rapid and substantial

* Corresponding author. State Key Laboratory of Magnetic Resonance and Atomic and Molecular Physics, Key Laboratory of Magnetic Resonance in Biological Systems, Wuhan Center for Magnetic Resonance, Wuhan Institute of Physics and Mathematics, Chinese Academy of Sciences, Wuhan, 430071, PR China.

** Corresponding author. University of Chinese Academy of Sciences, Beijing, 100049, PR China.

E-mail addresses: jie.wang@wipm.ac.cn (J. Wang), fuqiang.xu@wipm.ac.cn (F. Xu).

¹ These authors contributed equally to this work.

progress, particularly in mammals. Virus-based tracing is versatile as the target and spread properties of the virus can be modified. Many virus species have been utilized and manipulated for this purpose, such as rabies virus, vesicular stomatitis virus (VSV), herpes simplex virus (HSV), pseudorabies virus (PRV), adeno-associated virus (AAV), retrovirus, lentivirus, canine adenovirus (CAV), semliki forest virus, and Japanese encephalitis virus (Beier et al., 2011; Betley and Sternson, 2011; DeFalco et al., 2001; Ekstrand et al., 2008; Jia et al., 2016, 2017; Kelly and Strick, 2000; Lo and Anderson, 2011; Mazarakis et al., 2001; Salinas et al., 2009; Soudais et al., 2001; Ugolini, 2010; Wickersham et al., 2007), etc. The viruses available for neuronal circuit dissection universally rely on the fluorescent signal, and the detailed structures of the labeled neural cell bodies and fibers can clearly be viewed through fluorescent imaging. However, it is difficult to longitudinally investigate the neural circuit spread over a large brain area labeled for a given function or cell type using microscopic imaging.

On the other hand, as a non-invasive detection method, MRI has become an important tool for understanding the brains of humans and animals. MRI can offer insights into the structure, function, and metabolism of the brain (Rane et al., 2015), thus it has been widely used in scientific research and clinical applications in recent years. With the help of relevant MRI approaches, such as DTI (Mori and Zhang, 2006), and Manganese-enhanced magnetic resonance imaging (MEMRI) (Lin and Koretsky, 1997; Pautler et al., 1998; Silva et al., 2004), the neural networks can be predicted or detected. DTI-MRI produces information of the axonal organization of the entire brain (Le Bihan, 2003), however, it cannot provide information of anatomical connections through synapses. Mn²⁺ is anterogradely transported among synaptic connections, enabling the revelation of brain connectivity (Koretsky, 2012; Tucciarone et al., 2009; Zhang et al., 2010). Nevertheless, it is difficult to view the detailed structures of fibers and neurons with MEMRI, due to the limited spatial resolution in MRI. Therefore, it is valuable to develop a novel strategy that combines the advantages of neurotropic virus tracing and MRI approach.

As a metalloprotein (Cohen et al., 2007; Deans et al., 2006), ferritin is ubiquitous and highly conserved throughout most organisms (Arosio et al., 2009). It has a paramagnetic effect after bonding with iron in ferric (Fe³⁺) forms (Owen and Lindsay, 1983) and a marked effect on solvent NMR relaxation rates (Bulte et al., 1994; Gottesfeld and Neeman, 1996; Vymazal et al., 1998). Ferritin has been suggested as an MRI reporter for the detection of gene expression using MRI in several studies (Cohen et al., 2005, 2007; Genove et al., 2005; Iordanova and Ahrens, 2012). Replication-defective adenovirus (AdV) expressing ferritin can cause MRI contrast (T2 and T2*) in the brain (Genove et al., 2005), and AdV expressing a chimeric ferritin (light and heavy chain of ferritin fused by a linker, L*H) also enables the visualization of endogenous neuroblast migration in the brain from the subventricular zone towards the olfactory bulb (Iordanova and Ahrens, 2012). In a similar study, a lentiviral vector expressing ferritin was utilized and ferritin-labeled endogenous neural stem cell progeny was detected with MRI (Vande Velde et al., 2012). With lentiviral vector encoding ferritin and fluorescent proteins, tumors were detected by both ferritin based MRI and fluorescence imaging methods (Kim et al., 2010). However, ferritin encoding virus is rarely used to detect the neural connection. With the help of trans-synaptic neurotropic viruses and the MRI method, ferritin could become a potential element to visualize synaptically connected networks.

In this study, ferritin was coupled to enhanced green fluorescent protein (EGFP) gene and cloned into the VSV genome to generate a new trans-synaptic tracing tool. Our results demonstrate that the structural neural connection can be detected with both MRI and fluorescent imaging. Thus, this study provides a novel strategy which combines the methods of neurotropic virus tracing and MRI to visualize the labeled global network for a given type or function in the brain, whose precise anatomical connections through synapses can be verified through optical microimaging.

2. Materials and methods

2.1. Animal experiments

All animals involved in the experiments were treated in accordance with the protocols approved by the Animal Ethics Committee at the Wuhan Institute of Physics and Mathematics, Chinese Academy of Sciences (SYXK(E)2015–0051). All efforts were made to minimize animal suffering. Wild-type C57BL/6J mice were obtained from Hunan SJA Laboratory Animal Co., Ltd (Hunan, China). All the mice were kept in a 12h/12h light-dark cycle room (temperature, between 22 and 25 °C), and food and water were available *ad libitum*.

2.2. Virus construction

Due to biosafety issues, the *in vivo* MRI scans could only be conducted with replication-restricted rVSV-dG vectors, and the mice infected with rVSV vectors could not be used in the *in vivo* MRI study. Thus, there were four different kinds of viral vectors developed in the current study. 1) rVSV-dG-EGFP and rVSV-dG-Ferritin-EGFP: verify the virus expression of EGFP and detect the MRI signal of ferritin at the injection site in the *in vivo* MRI study; 2) rVSV-EGFP and rVSV-Ferritin-EGFP: check the trans-synaptic function of the viruses by optical imaging and detect the MRI signals of ferritin in multiple brain regions postmortem.

2.2.1. Plasmid construction

The Ferritin-t2a-EGFP fragment was amplified from pLV-CAG-mFerritin-EGFP plasmid (a gift from Prof. Xiaoming Li's lab in Zhejiang University). The chimeric ferritin gene (L*H) (from *Mus musculus*) and EGFP gene were linked with a 2A self-cleavable sequence (GCGGCGGGC GCGGCGGGCAGCGATTATAAAGATGATGATGA-TAAAGGCGGGCAGCGCGCGT), the fusion gene ((L*H)-t2a-EGFP fragment) was cloned into VSV vectors, rVSV-dG-EGFP (van den Pol et al., 2009) (Fig. 1A) and rVSV-EGFP (pVSV-Venus-VSVG) (Beier et al., 2011) (Fig. 2A) respectively, using XhoI and MscI cloning sites. In the virus genome, N, P, M, G and L are five VSV structural genes from a wild type virus, and G was deleted to construct a replication-restricted recombinant virus, rVSV-dG. The complete sequences of the recombinant constructs are shown in the supplementary materials.

2.2.2. Virus production

VSV viruses were rescued from plasmids as described in a previous study (Beier and Cepko, 2012). For the production of rVSV-Ferritin-EGFP, three T75 bottles of BHK cells at 95% confluency were infected at a MOI (multiplicity of infection) of 0.01. Viral supernatants were collected at 48 hpi. (hours post-infection) and ultra-centrifuged (50,000 g) using a JA25.25 rotor (Beckman Coulter, USA) and re-suspended with PBS in 0.1% of original volume. The concentrated viral stocks were titered in a dilution series to 100% confluent BHK cells and EGFP plaques were examined at 12 hpi. For the production of rVSV-dG-Ferritin-EGFP, 293T cells at 70% confluency on 10-cm dishes were transfected with 10 µg of pMD2.G (plasmid expressing VSVG) using FuGENE6 (Promega, USA). Twenty-four hours post-transfection, the cells were infected at a MOI of 0.01 with rVSV-dG-Ferritin-EGFP. Viral supernatants were collected at two dpi, then concentrated and the titer was determined as above. All viruses were stored at –80 °C for subsequent experiments.

2.3. Animal experiments

2.3.1. Animal surgery

Eight-week-old male C57BL/6 mice (20–25 g) were injected with the virus. The procedures of virus micro-injection are described in our previous study (Jia et al., 2016). Briefly, animals were anesthetized with chloral hydrate (400 mg/kg), and placed in a stereotaxic apparatus (Item: 68025 - stereotaxic apparatus and 68030 - mice adaptor, RWD, China).

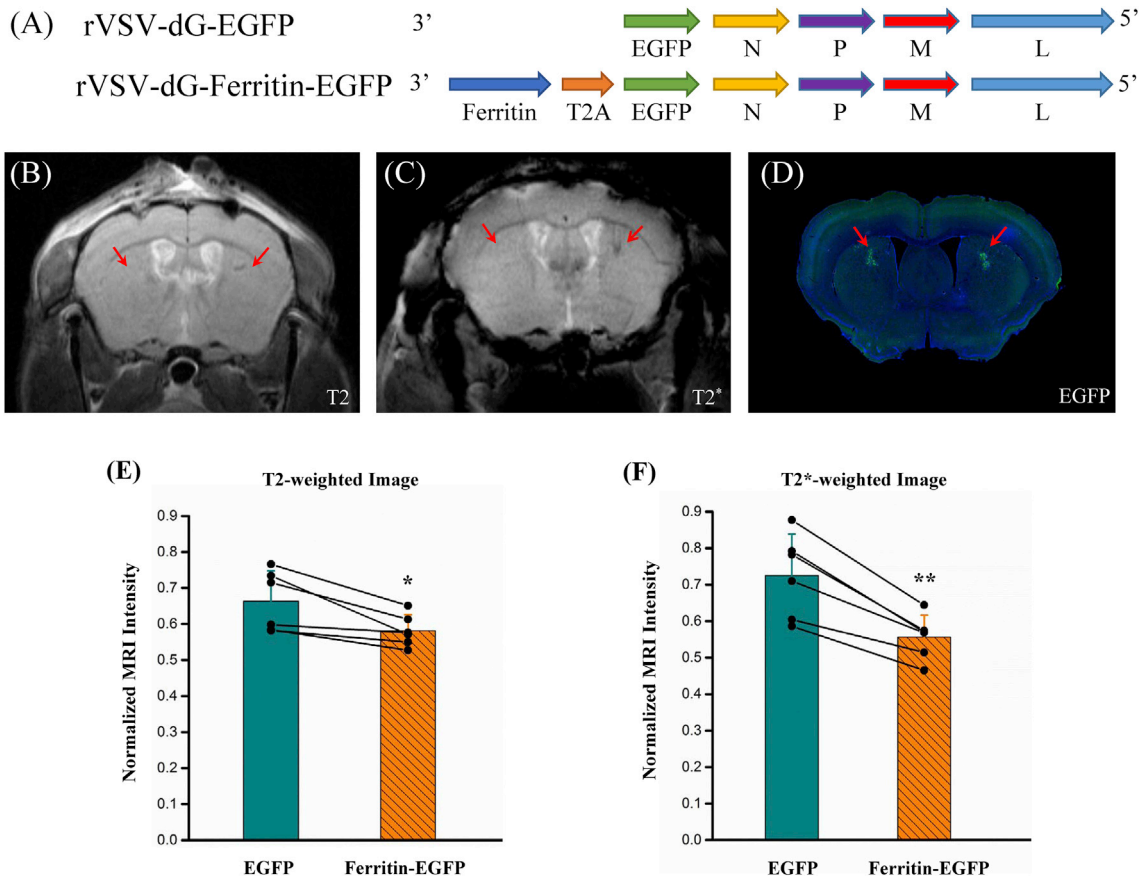


Fig. 1. Detection of ferritin delivered by replication-defective VSV with MRI in living animals (n = 6). *Note:* A: Virus genomes of rVSV-dG-EGFP and rVSV-dG-Ferritin-EGFP. N, P, M, G and L are five VSV structural genes from wild type viruses; G was deleted to construct a replication-restricted recombinant virus, VSV-dG (van den Pol et al., 2009); EGFP or Ferritin-EGFP gene was inserted into VSV-dG virus genome. B and C: Results of T2-weighted (B) and T2*-weighted (C) images seven days after injection (left arrows, rVSV-dG-EGFP; right arrow, rVSV-dG-Ferritin-EGFP); (D) Fluorescent image of the same slice from the same mouse. Comparison of the T2 (E) and T2* (F) Normalized T2 and T2* weighted MRI signals between brain regions infected with rVSV-dG-Ferritin-EGFP and rVSV-dG-EGFP, Paired t-test, Ave. ± STD; *: p 0.05; **: p 0.01.

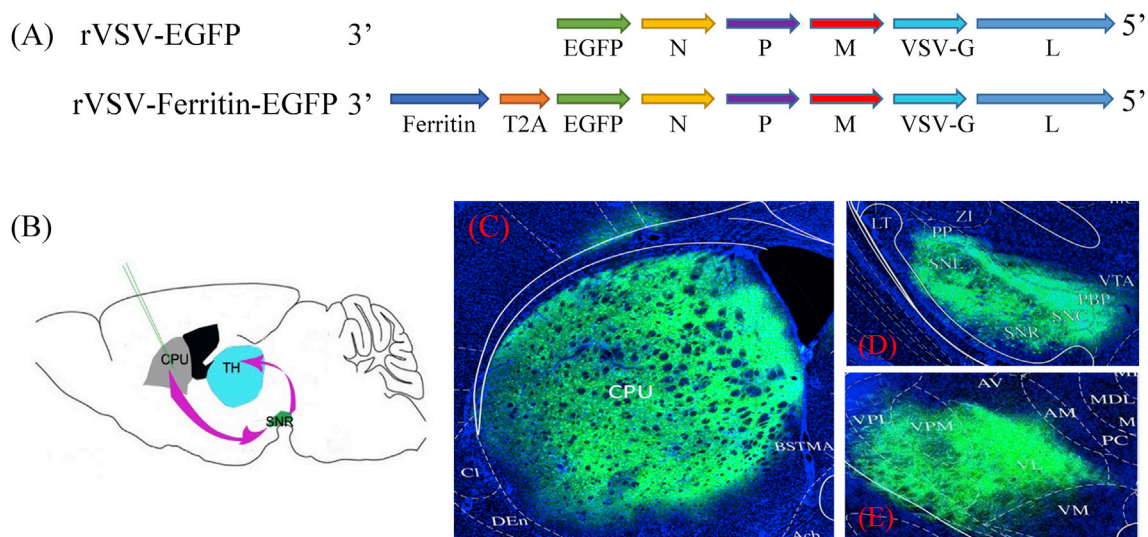


Fig. 2. rVSV-Ferritin-EGFP anterogradely transmitted across multiple synapses. *Note:* A: Virus genomes of rVSV-EGFP and rVSV-Ferritin-EGFP. N, P, M, G and L are five VSV structural genes from wild type viruses. EGFP or Ferritin-EGFP gene was inserted into VSV virus genome; B: rVSV-Ferritin-EGFP was microinjected into CPU; Expected targets for anterograde spread include SN (substantia nigra, primary anterograde trans-synaptic target) and TH (thalamus, secondary anterograde trans-synaptic target); C-E: The neurons in CPU, SN and TH were labeled with EGFP, suggesting that rVSV-Ferritin-EGFP spreads anterogradely along the synaptically connected network as expected.

The skull above the target area was thinned with a dental drill and removed carefully. The injections were conducted with a 10 µL syringe (Hamilton, Nevada, USA) connected with a glass micropipette (10–15 µm

diameter tip). The virus (100 nL, titer: 2E8) was stereotactically microinjected into the target region. In order to minimize diffusion, syringes were kept in place for 10 min after the injection was completed. The mice

that were injected with rVSVs (rVSV-Ferritin-EGFP, rVSV-EGFP, rVSV-dG-Ferritin-EGFP and rVSV-dG-EGFP) were kept in the Biosafety Level 2 (BSL-2) laboratory animal room.

For the target regions, two brain sites were selected: CPU (Caudate Putamen) (0.02 mm anterior to Bregma, 2 mm lateral from midline, 3 mm depth relative to Bregma) and SC (0.58 mm posterior to Bregma, 1.5 mm lateral from midline, 1.15 mm depth relative to Bregma). The region CPU was used for verifying the MRI contrast elicited by ferritin encoding VSV vector (rVSV-dG-Ferritin-EGFP) and trans-multisynaptic characteristic of rVSV-Ferritin-EGFP; the other region SC was used to detect and quantitatively analyze both the MRI and fluorescent signals of the trans-synaptic viruses (rVSV-Ferritin-EGFP: FerritinEGFP group; rVSV-EGFP: EGFP group) in different infected regions.

2.3.2. Sample collection

The rVSV-Ferritin-EGFP and rVSV-EGFP viruses (both replication competent) must be handled according to BSL-2 practices, which precluded use of the MRI scanner for imaging of live animals injected with these viruses. These samples were therefore prepared for *ex vivo* imaging. To monitor the virus-infected and iron loading procedures, the virus-infected mice were anaesthetized with an overdose of chloral hydrate three or four days after injection. Then the animals were perfused with 0.9% saline solution followed by 4% paraformaldehyde solution. The brain (with skull) was removed and imaged by the MRI scanner using the protocol in the following section. After the MRI study, the brain was removed from the skull and post-fixed over-night with 4% paraformaldehyde. The fixed brain was sectioned into 40 μ m slices with a microtome (Leica, German). For Perls' Prussian Blue staining, the brain slices were immersed in Perls' staining solution (Potassium ferrocyanide and hydrochloric acid - HCl, Solarbio, G1422, Beijing, China) for 45 min and cell nuclei were counterstained with nuclear fast red. For immunohistochemistry staining, the slices were incubated for 12 h at 4 °C with primary antibody (Abcam, ab69090, UK), washed and incubated for 2 h at 37 °C with Cy3-labeled secondary antibody. For fluorescent imaging, the brain slices were stained with DAPI and imaged by Olympus VS120 virtual microscopy slide scanning system (Olympus, Japan) and confocal microscope (Leica SP8, German).

2.3.3. MRI

MRI images were acquired from the brains of mice in a horizontal-bore 7.0 T BioSpec machine (Bruker, Ettlingen, Germany). A surface coil with a diameter of 20 mm was utilized in combination with a bird-cage transmit coil. Parameters included, the acquisition matrix size: 256 \times 196; the reconstruction matrix size: 256 \times 256; field of view (FOV): 2.0 cm \times 2.0 cm; and slice thickness: 0.5 mm. There were two kinds of MRI studies involved, *in vivo* and *ex vivo*. The other acquisition parameters for these two methods are respectively described as following:

For the *in vivo* MRI studies with living mice injected with rVSV-dG-Ferritin-EGFP and rVSV-dG-EGFP, coronal slices were acquired at the injection site using T2-weighted spin-echo (Rapid Acquisition with Relaxation Enhancement (RARE), TR/TE = 2,500/30–36 ms, rare factor = 4, echo spacing = 15–18 ms) and T2*-weighted gradient echo sequences (Fast Low Angle SHot (FLASH), TR/TE = 500/15–16.5 ms, Flip angles = 30°). As the contrast signals at the injection site were obviously observed, the echo time (TE) was not optimized during the scanning of living animals. The average number for T2-weighted imaging in living animals was set to 16, resulting in a total acquisition time of 32 min. The average number for T2*-weighted imaging in living animals was set to 9, resulting in a total acquisition time of 14 min. In order to avoid the motion artifacts during the scan, the animal was deeply anaesthetized, and the concentration of isoflurane was adjusted to 1.0–1.5%. The breath rate was controlled under 60 times/min. A warm water pad was utilized to maintain the body temperature of the animals (~37 °C).

According to the biological safety requirements for VSV, the living mice infected with rVSV-Ferritin-EGFP or rVSV-EGFP must not be

directly scanned using the MRI scanner. Thus, the virus-infected mice were perfused, and the brain (with skull) removed for the *ex vivo* MRI study. The *ex vivo* MRI scans for the intact brain were acquired using T2-weighted spin-echo sequence, and the average number was set to 16, resulting in the total acquisition time of 39 min. In order to improve the image quality for quantitative analysis, the parameters were optimized to TR/TE = 3,000/50 ms (RARE, rare factor = 4, echo spacing = 25 ms) for better T2 contrast and image quality.

2.4. Data processing

The procedures of analysis for fluorescence imaging and MRI are described separately:

For fluorescent images, the fluorescent signals in a given slice were automatically co-registered to the mice Allen brain atlas with a recently developed software (Agarwal et al., 2018), so as to reveal the locations of the fluorescent signals. In their method, 20 different ROIs were automatically recognized without distinguishing the left and right hemispheres. Thus, this ROI recognition method was not suitable for our work. In order to analyze the relationship between the MRI and fluorescent signals in different ROIs, the virus infected regions were manually traced out after the alignment of fluorescent images and brain atlas, and EGFP fluorescent signal intensities in the ROIs were extracted. Since all the optical imaging parameters were set the same and the green channel of the images were not overexposed, the green fluorescent signals were normalized using the highest value in all images.

For the *in vivo* MRI study, the rVSV-dG-Ferritin-EGFP infected area in the mice brain was manually drawn with Paravision 5.0 (Bruker Biospec, Germany), and the symmetrical site in the contralateral side was marked, then the MRI signals on both sides were collected for comparison. The MRI signal intensity of cerebrospinal fluid (CSF) in each animal was extracted and used as the reference to normalize the MRI signal intensity. (O'Neill et al., 2002; Tjoa et al., 2005).

For the *ex vivo* MRI study, the raw data was converted to nifti (hdr/img) format using Bruker2Analyze Converter (<http://people.cas.sc.edu/rorden/micro/bru2anz/>). The ferritin-expressing areas were segmented based on mouse brain MRI-T2 templates and atlas images. The atlas images of the mouse brain were constructed from the Paxinos and Franklin atlas figures, as described in our previous study (Nie et al., 2018). First, every individual image of the mouse brain was co-registered with a pair of brain template and brain atlas images, using the nearest interpolation method (Nie et al., 2013). Next, the spreading areas of ferritin encoding virus were identified by considering both the fluorescent signals and the difference between MRI signals in EGFP and FerritinEGFP groups, and the spreading areas of each mouse were manually traced out using MRICron (<https://www.nitrc.org/projects/mricron>) and saved as a mask image. Then, the overlapping voxels between the mask image and registered atlas image were determined. According to the sub-anatomical regional index in the atlas image, the spreading area of the ferritin encoding virus was segmented into several sub-anatomical regions. Finally, the mean voxel intensity in each sub-anatomical region was automatically calculated and normalized with MRI signal intensity in CSF. The following ROI were analyzed: Auditory cortex (AuC)_right (R), Caudate Putamen (CPU)_Left (L), CPU_R, Hippocampus (Hipp)_L, Hipp_R, Motor Cortex (MC)_L, MC_R, Retrosplenial cortex (RSC)_R, Somatosensory Cortex (SC)_L, SC_R, Thalamus (TH)_R, Visual Cortex (ViC)_R.

All of the data processing and analyses were implemented in MATLAB (MathWorks, Inc., USA).

2.5. Statistical analysis

All MRI signals were normalized with MRI signal intensity in cerebrospinal fluid (CSF). For comparison of the MRI signals in animals infected with rVSV-dG-EGFP and rVSV-dG-Ferritin-EGFP, a paired *t*-test was applied; the MRI signal and fluorescent signal intensities in the

FerritinEGFP and EGFP groups were compared with an independent student *t*-test (Two-tailed, $P < 0.05$). Results were presented in Average \pm Standard deviation (Ave. \pm STD).

3. Results

3.1. Effect of ferritin expressed by non-trans-synaptic VSV on MRI signal in living animals

Seven days after rVSV-dG-Ferritin-EGFP and the control virus (rVSV-dG-EGFP) were stereotactically microinjected into the right and left sides of CPU, respectively (Fig. 1A, $n = 6$), MRI studies were conducted in the living animals. The right injection site showed a robust contrast in both T2- and T2*-weighted images (Fig. 1B and C), while the left side did not. The fluorescent image of the same brain slice is shown in Fig. 1D, and it illustrates that the expression of the green fluorescence in the two injection sites are similar. The T2 and T2* weighted MRI signals were normalized with MRI signal intensity in CSF for comparison across subjects. The statistical results show that the brain region infected with rVSV-dG-Ferritin-EGFP had significantly reduced T2 (Fig. 1E, $p < 0.05$) and T2* (Fig. 1F, $p < 0.01$) weighted MRI signals. The results verified that ferritin expressed by rVSV-dG-Ferritin-EGFP could be used as an MRI contrast agent.

3.2. Trans-multi-synaptic property of rVSV-Ferritin-EGFP

The Ferritin-EGFP fused gene was cloned into a trans-multisynaptic tracing VSV system to construct a new recombinant virus, rVSV-Ferritin-EGFP (Fig. 2A), which probably spreads anterogradely along synaptic connections as rVSV-EGFP (Beier et al., 2011). rVSV-Ferritin-EGFP was stereotactically microinjected into CPU (Fig. 2B, $n = 2$). The mice were perfused and decapitated for MRI scanning and fluorescent imaging four days post-injection. The EGFP signals were detected in several regions including the injection site (Fig. 2C & Fig. S1). Among these regions, the substantia nigra (SN) and TH have been reported to be the primary and secondary anterograde targets of CPU, respectively (Fig. 2D and E) (Keeler et al., 2014). The results of fluorescent imaging show that the rVSV-Ferritin-EGFP could be utilized as an anterograde trans-multi-synaptic vector similar to rVSV-EGFP (Beier et al., 2011).

Changes of MRI T2 contrast were observed in CPU and SN (Fig. S2), but not in TH. This might be caused by multi-synapse connection between TH and CPU, and ferritin expressed by the virus in TH not having enough time to enrich Fe^{3+} . Furthermore, the location of TH was further away from the surface coil compared with SN (The surface coil was located at the bottom of the head). In order to obtain better imaging

quality and verify this novel strategy, first, another cortical region, SC, was selected in the following studies, and the surface coil was located dorsal to the brain (close to mouse cerebral cortex).

3.3. Detection of neural connections with ex vivo MRI and fluorescent imaging

Both trans-multi-synaptic virus tracers, rVSV-Ferritin-EGFP and rVSV-EGFP, were stereotactically microinjected into SC in two separated mice groups ($n = 5$ for each group) for both MRI and fluorescent imaging.

At first, three days after the injection, the mice were perfused and the brains (with skull) were subjected to the MRI scanner. There was overt T2 weighted MRI contrast in the local injection site, and only a few other brain regions seemed to show MRI contrast (Fig. S3), while green fluorescent signals were observed in many regions. Thus, the iron accumulation could be one of the important factors that influenced the MRI contrast.

Due to the cyto-toxicity of the replication complete VSV involved here (rVSV-EGFP and rVSV-Ferritin-EGFP), the infected animals died about four and a half days after the virus injection. So we chose to sacrifice the animals four days post-injection. Four days after the injection, the T2-weighted MRI images showed robust contrast in several brain regions in the FerritinEGFP group (rVSV-Ferritin-EGFP injected), while no discernable T2 contrast was found in the EGFP group (rVSV-EGFP injected) (Fig. 3). The darker MRI signal around the injection site in the EGFP group might be caused by tissue damage during the virus micro-injection procedure. The high-resolution images of the registration results of the fluorescent images and Allen Mouse Brain Connectivity Atlas (connectivity.brain-map.org) are provided in the supplemental material. (Fig. S4). The fluorescent images show that the green fluorescent signals were mainly distributed into 12 different brain regions - AuC_R, CPU_L, CPU_R, Hipp_L, Hipp_R, MC_L, MC_R, RSC_R, SC_L, SC_R, TH_R, ViC_R. These results also demonstrate that rVSV-EGFP and rVSV-Ferritin-EGFP mainly spread into the same brain regions.

Comparing the fluorescent and MRI images in the FerritinEGFP group, there is an extensive overlap between MRI contrast and EGFP signals in the virus infected brain regions. These results confirm that the MRI contrast in the T2-weighted image caused by ferritin in the rVSV-Ferritin-EGFP is detectable and traceable.

3.4. Comparing the results of MRI signals in FerritinEGFP and EGFP groups

In order to quantitatively analyze the MRI contrast caused by ferritin in the rVSV-Ferritin-EGFP, the normalized MRI signals between the FerritinEGFP and EGFP groups were compared. The MRI signals of 12

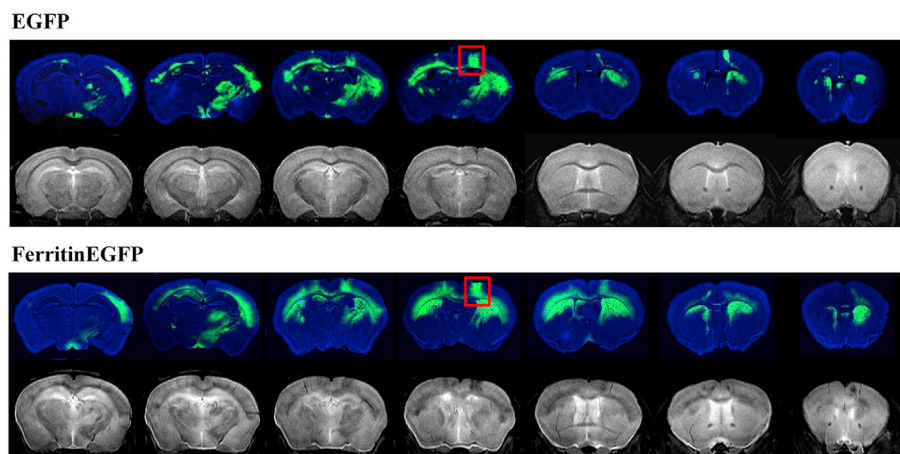


Fig. 3. The signals in MRI and fluorescent images in both rVSV-EGFP and rVSV-Ferritin-EGFP animals four days after the virus injection into the SC. Note: The brain (with skull) was removed and imaged with MRI scanner, and then the coronal slices were utilized for fluorescent imaging. Upper in both groups, fluorescent images; lower, MRI images; red box, the injection site.

brain regions that displayed obvious fluorescent signals in both groups were collected (Fig. 4). There was no virus infection in the Olfactory tubercle_R (OT_R) and OT_L, thus they were selected as control.

The T2-weighted MRI signals in the FerritinEGFP group were significantly lower (Fig. 4B, $p < 0.01$), which indicates that there was neuronal connectivity between these 11 virus-spreading brain regions and the virus injection site (SC_R). Due to the properties of the virus, these regions could be synaptically connected downstream regions of the SC_R. These results reveal that the rVSV-Ferritin-EGFP could be utilized as a trans-multi-synaptic neural circuit tracer using *ex vivo* MRI and fluorescent imaging approaches.

3.5. Immunohistochemistry and Perls' Prussian Blue staining

Immunohistochemistry was performed to detect ferritin expression and verify the co-localization of ferritin and EGFP. In the FerritinEGFP group, the ferritin and EGFP showed similar expression patterns and considerable signal overlaps in virus infected neurons (Figs. 5 and 6). Ferritin could cause the MRI contrast via the iron loading in its protein cage. In the FerritinEGFP group, Perls' Prussian Blue staining for iron (arrows) with Nuclear fast red counterstaining revealed the presence of Fe^{3+} in several brain regions (SC, CPU, Hipp, ViC and TH), in which all showed hypointense contrast in MRI images (Fig. 7A–H). OT was selected as the control region for comparison (Fig. 7I), where MRI signal was not significantly changed. There was lack of obvious Perls' Prussian Blue staining positive signal in OT. Furthermore, there was no overt iron accumulation in the control group (data not shown).

3.6. The relationship of MRI and fluorescent imaging signal intensities

In order to measure the efficiency of the MRI method for detecting the neural connections, the relationship of MRI contrast and green

fluorescent signal intensity in the FerritinEGFP group was analyzed. Because the neural connections with contralateral brain regions are more complicated, the injection site (SC_R) and seven ipsilateral brain regions with significant MRI contrast were included for the analysis of the correlation between MRI and fluorescent signals. Among these eight brain regions, the relationship between the green fluorescent signal intensity in the FerritinEGFP group and the ratio of the difference in normalized MRI signal intensities between groups (EGFP and FerritinEGFP) and the normalized MRI signal intensities in the EGFP group ($(S_{EGFP} - S_{FerritinEGFP}) / S_{EGFP}$, 'S' represents normalized MRI signal intensity) is illustrated (Fig. 8). According to the information in the Allen Mouse Brain Connectivity Atlas (connectivity.brain-map.org), all regions in Fig. 8 except Hipp_R receive direct projections from SC_R, which means that they are directly connected to the injection site. Thus, the time to accumulate iron in Hipp_R is different from other regions, which results in different MRI contrast. Therefore, linear regression analysis was applied for the rest six brain regions, $y = 0.4494x + 0.1302$ ($R^2 = 0.5904$). Besides, there was no significant difference in the fluorescent signal intensities of the selected ROIs in the groups of FerritinEGFP and EGFP (Fig. S5).

4. Discussion

Neural circuits are both extremely complex and exquisitely specific. Currently, neurotropic viral tracing is one of the most popular methods in neural circuitry exploration. Mostly, neurotropic viral tracers are viewed with microscopy imaging, which is not suitable for longitudinal investigation of the neural circuit. Here, our results demonstrate that structural neural connections could be detected using both *ex vivo* MRI and fluorescent imaging with the help of ferritin-EGFP fused gene encoding neurotropic viruses. The current strategy has the potential application of longitudinal monitoring of neural circuits in living animals. However, a few caveats, solutions and perspectives need to be discussed.

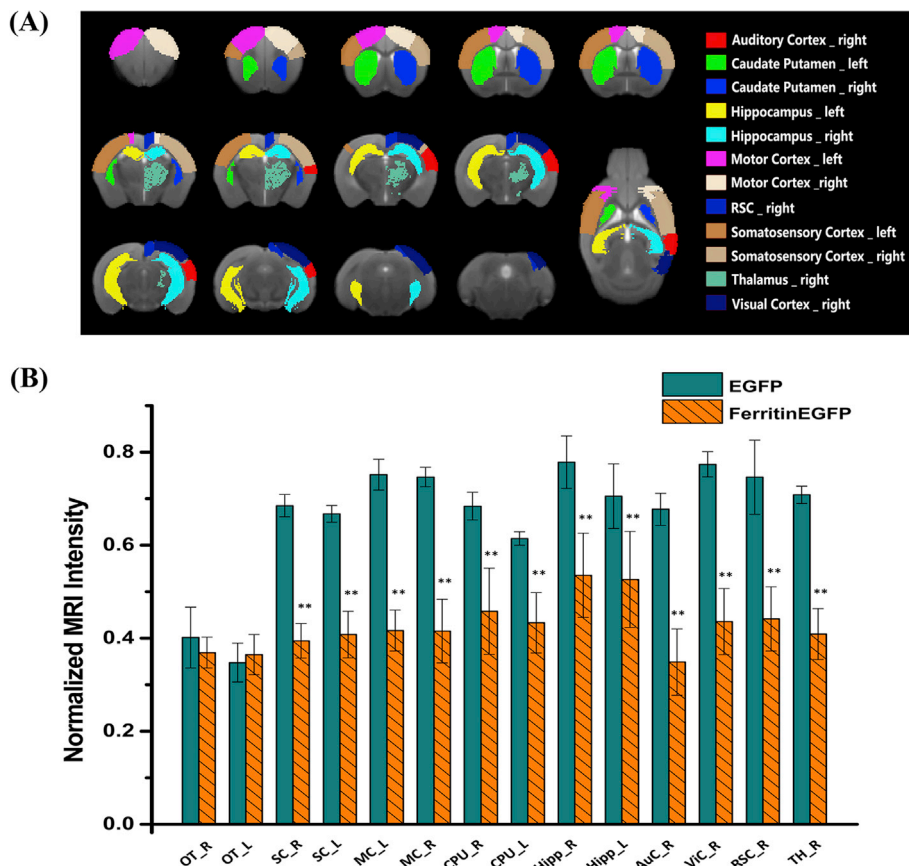


Fig. 4. Comparisons of the normalized MRI signals in the virus infected areas in the FerritinEGFP and EGFP groups. Note: A: Locations of the segmented selected regions (Auditory cortex (AuC_right (R), Caudate Putamen (CPU_Left (L), CPU_R, Hippocampus (Hipp)_L, Hipp_R, Motor Cortex (MC)_L, MC_R, RSC_R, Somatosensory Cortex (SC)_L, SC_R, Thalamus (TH)_R, Visual Cortex (ViC)_R) on the structural MRI images; B: Comparisons of the normalized MRI signals in the virus infected areas, Olfactory tubercle_R (OT_R) and OT_L which were selected as control. Note: * $p < 0.05$, ** $p < 0.01$, two-tailed *t*-test, Ave. \pm STD, $n = 5$.

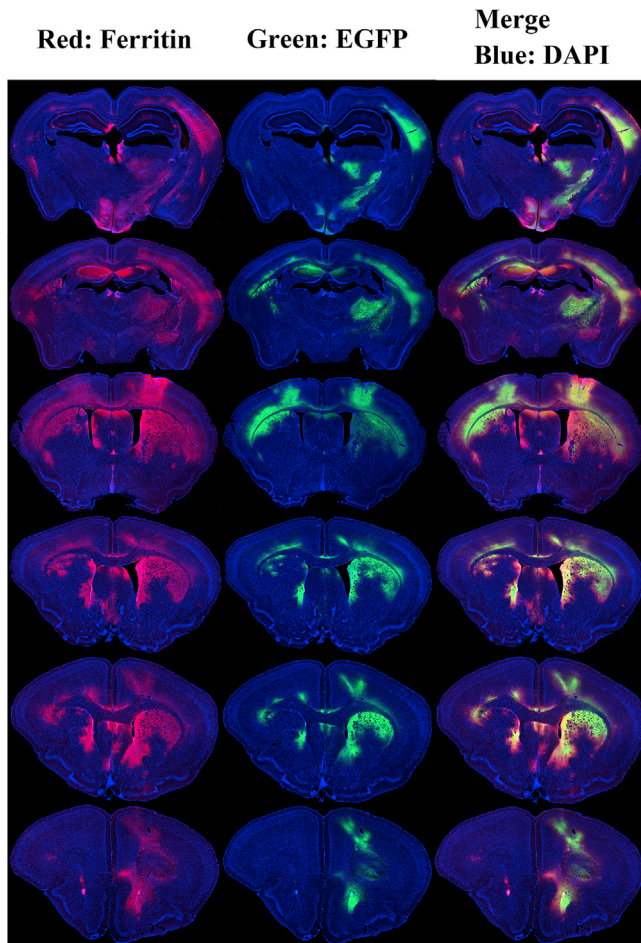


Fig. 5. Co-localization of ferritin and EGFP proteins in brain regions infected with rVSV-Ferritin-EGFP. Note: Immunohistochemistry staining demonstrates that ferritin (Red) and EGFP (Green) proteins express similar patterns in FerritinEGFP group. The cell nuclei (Blue) were counterstained with DAPI.

4.1. Explanation of T2 hypointense contrast caused by Ferritin encoding virus

The optical measurement is mostly influenced by the expression level of EGFP. However, multiple confounding factors affect the ferritin-based

MRI signal. The signal could be influenced by cellular iron loading, which is determined by a few factors, including the level of ferritin expressed in the infected neurons, the iron enrichment capability of the infected neurons, the availability of iron ions, and the duration of the enrichment period. Other factors related to imaging signals include the distance between the infected regions and the surface coil, and the state of the imaging system such as shimming quality.

It is difficult to optimize all these experimental parameters to quantitatively resolve explicit relationships between the MRI signals and the ferritin encoding trans-synaptic virus infection in different brain regions. There were eight ipsilateral virus infected brain regions involved in the current study (Fig. 8). The injection site, SC_R, showed the highest EGFP fluorescent signal intensity, unlike its MRI contrast. This could be caused by the operation damage and inflammation at the injection site of both groups. The region Hipp_R is not directly connected to the injection site – SC_R, and there was less time for the ferritin expressed in Hipp_R to enrich iron, thus, the difference of MRI signal intensity may be correspondingly weak. Among the rest of the regions, the difference in normalized MRI signal intensity increased following the rise of green fluorescent signal intensity, which indicates that more ferritin-EGFP expressed in the virus infected neurons resulted in stronger MRI contrast. Anyway, more efforts to elucidate the complex relationship between the MRI signals and ferritin encoding trans-synaptic virus infection is ongoing.

4.2. Application of other kinds of MRI reporters

In the current study, ferritin was cloned into VSV to generate a modified virus in order to investigate the neural connections in the brain. Other kinds of MRI reporter genes could be delivered by trans-synaptic viruses for neural circuit tracing systems. Currently, there are a number of MRI reporters (Kang and Chung, 2008; Mukherjee et al., 2016; Ray et al., 2003; Weissleder et al., 1997), such as transferrin receptor (Kang and Chung, 2008; Weissleder et al., 2000), beta-galactosidase (Louie et al., 2000), MagA (Zurkiya et al., 2008), Tyrosinase (Alfke et al., 2003; Weissleder et al., 1997), LRP (Gilad et al., 2007), and human aquaporin 1 (AQP1) (Mukherjee et al., 2016). These modified tools could be detected using different kinds of MRI methods, such as T2 and T2* (transferrin receptor, beta-galactosidase and MagA), T1 (Tyrosinase), CEST (Chemical Exchange Saturation Transfer: LRP), or DWI (AQP1).

4.3. Limitation and perspective

According to the biological safety requirements of VSV, this related in

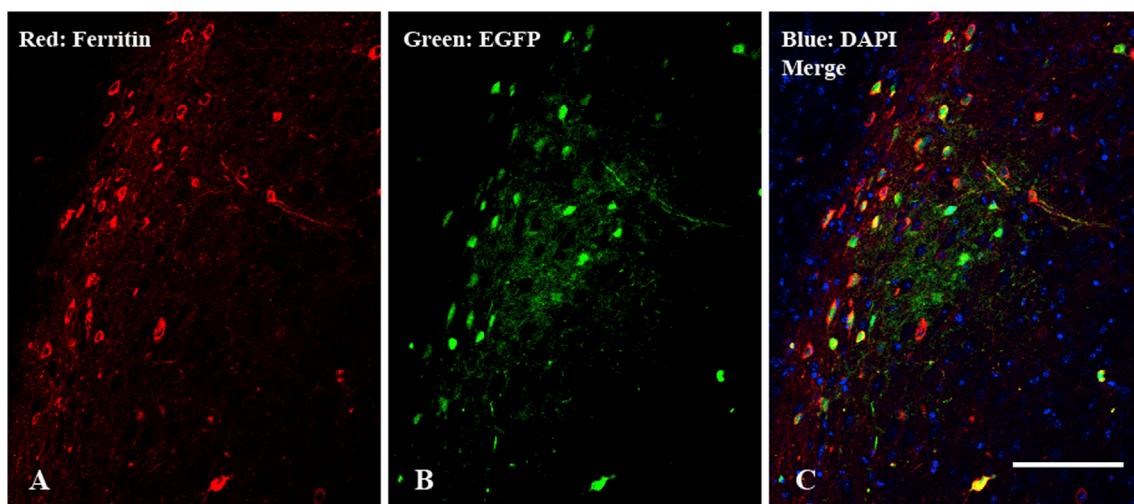


Fig. 6. Confocal image of AuC in FerritinEGFP group shows that ferritin (Red) colocalized with EGFP (Green) protein. Note: The cell nuclei (Blue) were counterstained with DAPI. Scale bar = 100 μ m.

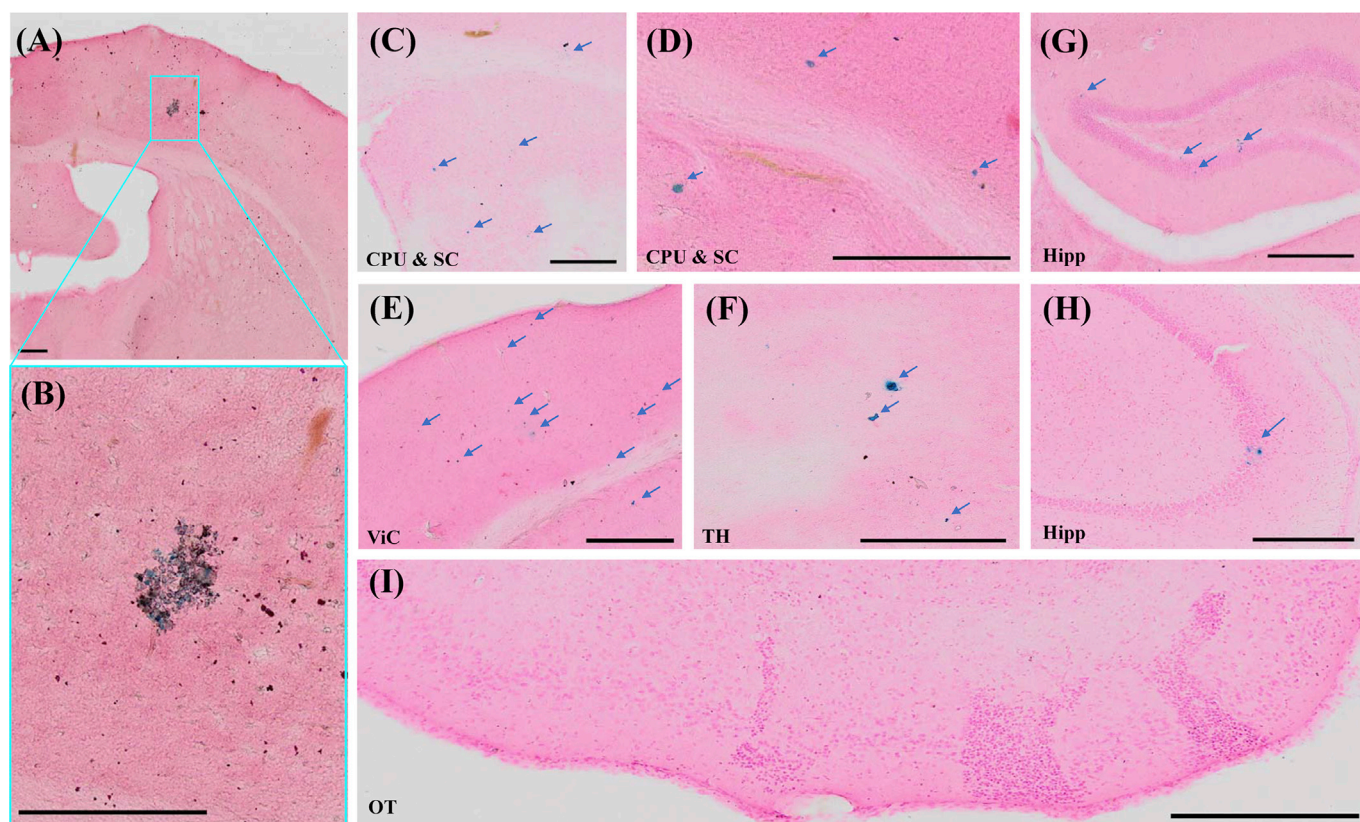


Fig. 7. Increased iron accumulation in brain regions infected with rVSV-Ferritin-EGFP. Note: A-B: In FerritinEGFP group, Perls' Prussian Blue staining reveals obvious iron accumulation in the injection site. C-H: Presence of Fe^{2+} in several brain regions (SC, CPU, Hipp, ViC and TH) that displayed hypointense contrast in MRI images. I: OT was selected as the control region for comparison, where MRI signal was not significantly changed. There was lack of obvious positive Perls' Prussian Blue staining positive area in OT. Scale bar = 300 μ m.

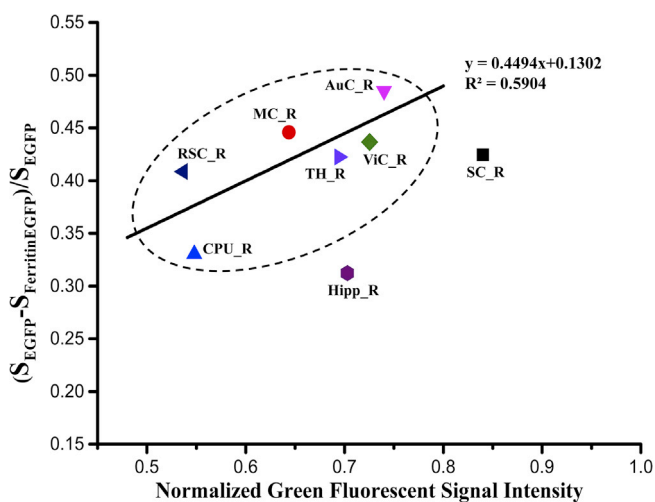


Fig. 8. The relationship between the green fluorescent signal intensity in the FerritinEGFP group and the ratio of the difference in normalized MRI signal intensities between groups (EGFP and FerritinEGFP) and the normalized MRI signal intensities in the EGFP group ($(S_{EGFP} - S_{FerritinEGFP}) / S_{EGFP}$). Note: A linear trend line was drawn for RSC_R, CPU_R, MC_R, AuC_R, TH_R and ViC_R, $y = 0.4494x + 0.1302$ ($R^2 = 0.5904$).

in vivo study should be conducted in the BSL-2 laboratory, and the living mice infected with rVSV cannot be directly scanned using the MRI scanner. Thus, the virus-infected mice were perfused, and the brain (with skull) was removed for *ex vivo* MRI study. However, this study provided a novel concept to directly detect the neural connection using MRI method, and it also has a potential ability to longitudinally trace the neural circuit.

There are different strategies to overcome the limitation that *in vivo* MRI study is not allowed for rVSV infected mice. It is possible to construct a micro-isolation system that satisfies the BSL-2 environment and is compatible with MRI scanner for *in vivo* MRI imaging of VSV infected mice in future study. With the help of other kinds of ferritin encoding neurotropic viruses, the neural circuitry with different spread directions or cascade of synaptic connections could be dissected. If ferritin is cloned into this monosynaptic labeling system, the direct output of the type-specific start neurons might be detected by the MRI T2-weighted image. Using a similar method, the PRV system carrying ferritin could provide the input of the starting neurons with MRI. Furthermore, CAV or rAAV2-retro with ferritin could map the direct input of the start neurons using the same approach (Soudais et al., 2001; Tervo et al., 2016). Development of a new tracing system and toxicity attenuation of VSV, PRV and HSV have been included in ongoing projects in the laboratory.

A more attractive alternative is to develop new toxicity attenuated viruses which could be used to trace neural circuits in live animals using a normal MRI scanner. In the current study, VSV was utilized to label the neurons at the injection site and the multi-step outputs from the starting area, as it spread exclusively anterogradely in neural circuit (Beier et al., 2011). With the help of other kinds of ferritin encoding neurotropic viruses, the neural circuitry with different spread directions or cascade of synaptic connections could be dissected. If ferritin is cloned into this monosynaptic labeling system, the direct output of the type-specific start neurons might be detected by the MRI T2-weighted image. Using a similar method, the PRV system carrying ferritin could provide the input of the starting neurons with MRI. Furthermore, CAV or rAAV2-retro with ferritin could map the direct input of the start neurons using the same approach (Soudais et al., 2001; Tervo et al., 2016). Development of a new tracing system and toxicity attenuation of VSV, PRV and HSV have been included in ongoing projects in the laboratory.

In the future, with the development of attenuated virus, which is a challenge when detecting neural circuit in live animals, the neural circuit could be observed longitudinally. During future live animal studies, the MRI detection conditions could be similar to the method used in Fig. 1. The MRI scanning parameters such as repetition time and echo time could be optimized for better signal noise ratio and T2 contrast. Therefore, this approach has the potential application to longitudinally trace the neural circuit in live animals.

5. Conclusion

To summarize, the advantages of neurotropic virus based neural circuit tracing and MRI technology were combined together in this new strategy, which enabled the detection of the neural connection using both *ex vivo* MRI and fluorescent imaging. The MRI reporter gene ferritin was cloned into the VSV system and sufficiently elicited MRI contrast in the T2-weighted image. After the virus injection, propagation and transsynaptic transmission, MRI contrasts and EGFP signals were observed in the same brain regions. This method exhibits the neural connection through MRI detection and allows high-resolution microscopy detection of fine structures in neural pathways, which bridge the observation of neural connections from macroscopic and microscopic scales. The strategy of the current study has the potential to investigate neural circuits in live animals.

Acknowledgement

The authors would like to express their gratitude to Graeme F. Mason (Yale University, USA) for the help of discussion and manuscript writing; Mr. Hansen Wu (Vanderbilt University, USA) and Bruno Hamish Unger (University of Otago, New Zealand) for the proofreading; Dr. Nitin Agarwal (University of California) for providing the program (Agarwal et al., 2018) for registration of fluorescent images and mice brain atlas; Dr. Zhengwu Zhang (University of Rochester) for performing the fluorescent image registration.

Appendix A. Supplementary data

Supplementary data related to this article can be found at <https://doi.org/10.1016/j.neuroimage.2019.04.039>.

Funding

This work was supported by the Chinese Ministry of Science and Technology (2015CB755601, 2015AA020508); the Chinese Academy of Science (XDB02050005); and the National Natural Science Foundation of China (31400976) and the Youth Innovation Promotion Association of Chinese Academy of Sciences (Y6Y0021004).

Financial Disclosures

The authors report no biomedical financial interests or potential conflicts of interest.

References

- Agarwal, N., Xu, X., Gopi, M., 2018. Geometry processing of conventionally produced mouse brain slice images. *J. Neurosci. Methods* 306, 45–56.
- Alfke, H., Stöppler, H., Nocken, F., Heverhagen, J.T., Kleb, B., Czubayko, F., Klose, K.J., 2003. In vitro MR imaging of regulated gene expression. *Radiology* 228, 488–492.
- Arosio, P., Ingrassia, R., Cavadini, P., 2009. Ferritins: a family of molecules for iron storage, antioxidation and more. *Biochim. Biophys. Acta* 1790, 589–599.
- Beier, K., Cepko, C., 2012. Viral tracing of genetically defined neural circuitry. *J. Vis. Exp.* 68, e4253.
- Beier, K.T., Saunders, A., Oldenburg, I.A., Miyamichi, K., Akhtar, N., Luo, L., Whelan, S.P., Sabatini, B., Cepko, C.L., 2011. Anterograde or retrograde transsynaptic labeling of CNS neurons with vesicular stomatitis virus vectors. *Proc. Natl. Acad. Sci. U. S. A.* 108, 15414–15419.
- Betley, J.N., Sternson, S.M., 2011. Adeno-associated viral vectors for mapping, monitoring, and manipulating neural circuits. *Hum. Gene Ther.* 22, 669–677.
- Brog, J.S., Salyapongse, A., Deutch, A.Y., Zahm, D.S., 1993. The patterns of afferent innervation of the core and shell in the accumbens part of the rat ventral striatum - immunohistochemical detection of retrogradely transported fluorogold. *J. Comp. Neurol.* 338, 255–278.
- Bulte, J.W.M., Douglas, T., Mann, S., Frankel, R.B., Moskowitz, B.M., Brooks, R.A., Baumgarner, C.D., Vymazal, J., Strub, M.P., Frank, J.A., 1994. Magnetoferritin - characterization of a novel superparamagnetic Mr contrast agent. *J. Magn. Reson. Imaging* 4, 497–505.
- Callaway, E.M., 2008. Transneuronal circuit tracing with neurotropic viruses. *Curr. Opin. Neurobiol.* 18, 617–623.

- Cohen, B., Dafni, H., Meir, G., Harmelin, A., Neeman, M., 2005. Ferritin as an endogenous MRI reporter for noninvasive imaging of gene expression in C6 glioma tumors. *Neoplasia* 7, 109–117.
- Cohen, B., Ziv, K., Plaks, V., Israely, T., Kalchenko, V., Harmelin, A., Benjamin, L.E., Neeman, M., 2007. MRI detection of transcriptional regulation of gene expression in transgenic mice. *Nat. Med.* 13, 498–503.
- Deans, A.E., Wadghiri, Y.Z., Bernas, L.M., Yu, X., Rutt, B.K., Turnbull, D.H., 2006. Cellular MRI contrast via coexpression of transferrin receptor and ferritin. *Magn. Reson. Med.* 56, 51–59.
- DeFalco, J., Tomishima, M., Liu, H., Zhao, C., Cai, X., Marth, J.D., Enquist, L., Friedman, J.M., 2001. Virus-assisted mapping of neural inputs to a feeding center in the hypothalamus. *Science* 291, 2608–2613.
- Ekstrand, M.I., Enquist, L.W., Pomeranz, L.E., 2008. The alpha-herpesviruses: molecular pathfinders in nervous system circuits. *Trends Mol. Med.* 14, 134–140.
- Enquist, L.W., Card, J.P., 2003. Recent advances in the use of neurotropic viruses for circuit analysis. *Curr. Opin. Neurobiol.* 13, 603–606.
- Genove, G., DeMarco, U., Xu, H., Goins, W.F., Ahrens, E.T., 2005. A new transgene reporter for *in vivo* magnetic resonance imaging. *Nat. Med.* 11, 450–454.
- Gilad, A.A., McMahon, M.T., Walczak, P., Winnard, P.T., Raman, V., van Laarhoven, H.W.M., Skoglund, C.M., Bulte, J.W.M., van Zijl, P.C.M., 2007. Artificial reporter gene providing MRI contrast based on proton exchange. *Nat. Biotechnol.* 25, 217–219.
- Gottesfeld, Z., Neeman, M., 1996. Ferritin effect on the transverse relaxation of water: NMR microscopy at 9.4 T. *Magn. Reson. Med.* 35, 514–520.
- Horowitz, L.F., Montmayeur, J.P., Echeleard, Y., Buck, L.B., 1999. A genetic approach to trace neural circuits. *Proc. Natl. Acad. Sci. U. S. A.* 96, 3194–3199.
- Iordanova, B., Ahrens, E.T., 2012. *In vivo* magnetic resonance imaging of ferritin-based reporter visualizes native neuroblast migration. *Neuroimage* 59, 1004–1012.
- Jia, F., Miao, H., Zhu, X.T., Xu, F.Q., 2017. Pseudo-typed Semliki Forest virus delivers EGFP into neurons. *J. Neurovirol.* 23, 205–215.
- Jia, F., Zhu, X., Xu, F., 2016. A single adaptive point mutation in Japanese encephalitis virus capsid is sufficient to render the virus as a stable vector for gene delivery. *Virology* 490, 109–118.
- Kang, J.H., Chung, J.K., 2008. Molecular-genetic imaging based on reporter gene expression. *J. Nucl. Med.* 49, 164s–179s.
- Keeler, J.F., Pretsell, D.O., Robbins, T.W., 2014. Functional implications of dopamine D1 vs. D2 receptors: a 'prepare and select' model of the striatal direct vs. indirect pathways. *Neuroscience* 282, 156–175.
- Kelly, R.M., Strick, P.L., 2000. Rabies as a transneuronal tracer of circuits in the central nervous system. *J. Neurosci. Methods* 103, 63–71.
- Kim, H.S., Cho, H.R., Choi, S.H., Woo, J.S., Moon, W.K., 2010. *In vivo* imaging of tumor transduced with bimodal lentiviral vector encoding human ferritin and green fluorescent protein on a 1.5T clinical magnetic resonance scanner. *Cancer Res.* 70, 7315–7324.
- Koretsky, A.P., 2012. Is there a path beyond BOLD? Molecular imaging of brain function. *Neuroimage* 62, 1208–1215.
- Lai, B.Q., Qiu, X.C., Zhang, K., Zhang, R.Y., Jin, H., Li, G., Shen, H.Y., Wu, J.L., Ling, E.A., Zeng, Y.S., 2015. Cholera toxin B subunit shows transneuronal tracing after injection in an injured sciatic nerve. *PLoS One* 10.
- Le Bihan, D., 2003. Looking into the functional architecture of the brain with diffusion MRI. *Nat. Rev. Neurosci.* 4, 469–480.
- Lerner, T.N., Ye, L., Deisseroth, K., 2016. Communication in neural circuits: tools, opportunities, and challenges. *Cell* 164, 1136–1150.
- Lin, Y.J., Koretsky, A.P., 1997. Manganese ion enhances T1-weighted MRI during brain activation: an approach to direct imaging of brain function. *Magn. Reson. Med.* 38, 378–388.
- Lo, L., Anderson, D.J., 2011. A Cre-dependent, anterograde transsynaptic viral tracer for mapping output pathways of genetically marked neurons. *Neuron* 72, 938–950.
- Louie, A.Y., Huber, M.M., Ahrens, E.T., Rothbacher, U., Moats, R., Jacobs, R.E., Fraser, S.E., Meade, T.J., 2000. *In vivo* visualization of gene expression using magnetic resonance imaging. *Nat. Biotechnol.* 18, 321–325.
- Mazarakis, N.D., Azzouz, M., Rohlf, J.B., Ellard, F.M., Wilkes, F.J., Olsen, A.L., Carter, E.E., Barber, R.D., Baban, D.F., Kingsman, S.M., Kingsman, A.J., O'Malley, K., Mitrophanous, K.A., 2001. Rabies virus glycoprotein pseudotyping of lentiviral vectors enables retrograde axonal transport and access to the nervous system after peripheral delivery. *Hum. Mol. Genet.* 10, 2109–2121.
- Mori, S., Zhang, J., 2006. Principles of diffusion tensor imaging and its applications to basic neuroscience research. *Neuron* 51, 527–539.
- Mukherjee, A., Wu, D., Davis, H.C., Shapiro, M.G., 2016. Non-invasive imaging using reporter genes altering cellular water permeability. *Nat. Commun.* 7.
- Nie, B., Chen, K., Zhao, S., Liu, J., Gu, X., Yao, Q., Hui, J., Zhang, Z., Teng, G., Zhao, C., Shan, B., 2013. A rat brain MRI template with digital stereotaxic atlas of fine anatomical delineations in paxinos space and its automated application in voxel-wise analysis. *Hum. Brain Mapp.* 34, 1306–1318.
- Nie, B., Wu, D., Liang, S., Liu, H., Sun, X., Li, P., Huang, Q., Zhang, T., Feng, T., Ye, S., Zhang, Z., Shan, B., 2018. A stereotaxic MRI template set of mouse brain with fine sub-anatomical delineations: application to MEMRI studies of 5XFAD mice. *Magn. Reson. Imaging* 57, 83–94.
- Numan, M., Numan, M.J., 1997. Projection sites of medial preoptic area and ventral bed nucleus of the stria terminalis neurons that express Fos during maternal behavior in female rats. *J. Neuroendocrinol.* 9, 369–384.
- O'Neill, J., Schuff, N., Marks, W.J., Feiwel, R., Aminoff, M.J., Weiner, M.W., 2002. Quantitative H-1 magnetic resonance spectroscopy and MRI of Parkinson's disease. *Mov. Disord.* 17, 917–927.
- Owen, C.S., Lindsay, J.G., 1983. Ferritin as a label for high-gradient magnetic separation. *Biophys. J.* 42, 145–150.

- Paton, J.A., Nottebohm, F., 1984. Neurons generated in the adult brain are recruited into functional circuits. *Science* 225, 1046–1048.
- Pautler, R.G., Silva, A.C., Koretsky, A.P., 1998. In vivo neuronal tract tracing using manganese-enhanced magnetic resonance imaging. *Magn. Reson. Med.* 40, 740–748.
- Rane, P., Cochran, D., Hodge, S.M., Haselgrove, C., Kennedy, D.N., Frazier, J.A., 2015. Connectivity in autism: a review of MRI connectivity studies. *Harv. Rev. Psychiatry* 23, 223–244.
- Ray, P., Wu, A.M., Gambhir, S.S., 2003. Optical bioluminescence and positron emission tomography imaging of a novel fusion reporter gene in tumor xenografts of living mice. *Cancer Res.* 63, 1160–1165.
- Salinas, S., Bilsland, L.G., Henaff, D., Weston, A.E., Keriell, A., Schiavo, G., Kremer, E.J., 2009. CAR-associated vesicular transport of an adenovirus in motor neuron axons. *PLoS Pathog.* 5, e1000442.
- Silva, A.C., Lee, J.H., Aoki, I., Koretsky, A.P., 2004. Manganese-enhanced magnetic resonance imaging (MEMRI): methodological and practical considerations. *NMR Biomed.* 17, 532–543.
- Soudais, C., Laplace-Builhe, C., Kissa, K., Kremer, E.J., 2001. Preferential transduction of neurons by canine adenovirus vectors and their efficient retrograde transport in vivo. *FASEB (Fed. Am. Soc. Exp. Biol.) J.* 15, 2283–2285.
- Tervo, D.G., Hwang, B.Y., Viswanathan, S., Gaj, T., Lavzin, M., Ritola, K.D., Lindo, S., Michael, S., Kuleshova, E., Ojala, D., Huang, C.C., Gerfen, C.R., Schiller, J., Dudman, J.T., Hantman, A.W., Looger, L.L., Schaffer, D.V., Karpova, A.Y., 2016. A designer AAV variant permits efficient retrograde access to projection neurons. *Neuron* 92, 372–382.
- Tjoa, C.W., Benedict, R.H.B., Weinstock-Guttman, B., Fabiano, A.J., Bakshi, R., 2005. MRI T2 hypointensity of the dentate nucleus is related to ambulatory impairment in multiple sclerosis. *J. Neurol. Sci.* 234, 17–24.
- Tuciarone, J., Chuang, K.H., Dodd, S.J., Silva, A., Pelled, G., Koretsky, A.P., 2009. Layer specific tracing of corticocortical and thalamocortical connectivity in the rodent using manganese enhanced MRI. *Neuroimage* 44, 923–931.
- Tye, K.M., Deisseroth, K., 2012. Optogenetic investigation of neural circuits underlying brain disease in animal models. *Nat. Rev. Neurosci.* 13, 251–266.
- Ugolini, G., 2010. Advances in viral transneuronal tracing. *J. Neurosci. Methods* 194, 2–20.
- van den Pol, A.N., Ozduman, K., Wollmann, G., Ho, W.S., Simon, I., Yao, Y., Rose, J.K., Ghosh, P., 2009. Viral strategies for studying the brain, including a replication-restricted self-amplifying delta-G vesicular stomatitis virus that rapidly expresses transgenes in brain and can generate a multicolor golgi-like expression. *J. Comp. Neurol.* 516, 456–481.
- Vande Velde, G., Raman Rangarajan, J., Vreys, R., Guglielmetti, C., Dresselaers, T., Verhoye, M., Van der Linden, A., Debyser, Z., Baekelandt, V., Maes, F., Himmelreich, U., 2012. Quantitative evaluation of MRI-based tracking of ferritin-labeled endogenous neural stem cell progeny in rodent brain. *Neuroimage* 62, 367–380.
- Vymazal, J., Brooks, R.A., Bulte, J.W.M., Gordon, D., Aisen, P., 1998. Iron uptake by ferritin: NMR relaxometry studies at low iron loads. *J. Inorg. Biochem.* 71, 153–157.
- Weissleder, R., Moore, A., Mahmood, U., Bhorade, R., Benveniste, H., Chioocca, E.A., Basilion, J.P., 2000. In vivo magnetic resonance imaging of transgene expression. *Nat. Med.* 6, 351–355.
- Weissleder, R., Simonova, M., Bogdanova, A., Bredow, S., Enochs, W.S., Bogdanov, A., 1997. MR imaging and scintigraphy of gene expression through melanin induction. *Radiology* 204, 425–429.
- Wickersham, I.R., Lyon, D.C., Barnard, R.J., Mori, T., Finke, S., Conzelmann, K.K., Young, J.A., Callaway, E.M., 2007. Monosynaptic restriction of transsynaptic tracing from single, genetically targeted neurons. *Neuron* 53, 639–647.
- Zhang, X.W., Bearer, E.L., Boulat, B., Hall, F.S., Uhl, G.R., Jacobs, R.E., 2010. Altered neurocircuitry in the dopamine transporter knockout mouse brain. *PLoS One* 5.
- Zurkiya, O., Chan, A.W., Hu, X., 2008. MagA is sufficient for producing magnetic nanoparticles in mammalian cells, making it an MRI reporter. *Magn. Reson. Med.* 59, 1225–1231.